An Insight into the Mechanism and Kinetics of Reactions In BOF Steelmaking: Theory vs Practice

A. K. Shukla[1)*], B. Deo[1)], S. Millman[2)], B. Snoeijer[2)], A. Overbosch[2)], and A. Kapilashrami[2)]

[1)] Department of Materials Science and Engineering, Indian Institute of Technology, Kanpur, 208016, India
[2)] Tata Steel Research, Development & Technology, PO Box 10.000, 1970 CA IJmuiden, The Netherlands
* Corresponding author; e-mail: shukla@iitk.ac.in

A thermodynamic (equilibrium) model is developed for the BOF process. The predictions of this model show the trend of reactions when the process is considered to be at thermodynamic equilibrium. In the case of a real process, however, some tuning and adaptation becomes necessary to make more accurate predictions. A dynamic model is developed in which the kinetics of scrap dissolution is also incorporated. A comparison of the results of the equilibrium and dynamic models (made with some tuning parameters) reveals that mixing is the prime factor which can alter the course of reaction at any particular instant. Mixing is greatly affected by oxygen flow rate, lance height and the nature of scrap. The understanding of the secrets of process dynamics becomes clearer with this approach, providing a good insight into the process.

Keywords: thermodynamics, Gibb's free energy, mathematical model, BOF steelmaking

Submitted on 15 March 2010, accepted on 31 May 2010

Introduction

The modeling of reactions in BOF steel making has been a topic of keen theoretical and practical interest over last several decades and the literature is replete with both laboratory and plant investigations [1–23]. In the present work the focus is essentially on decarburization reaction in the middle blow period of BOF.

The decarburization reaction in BOF has been investigated by several workers in the past [1, 2]. It has been suggested that decarburization may take place in the slag-metal emulsion, directly under the jet, on the refractory walls and within the CO gas bubbles rising in the bulk metal. In the earlier works, the slag-metal emulsion was considered to play a dominant role in decarburization. It was assumed that decarburization proceeded through the following intermediate steps:

1. Ejection of metal droplets into the slag phase due to (a) the effect of impinging oxygen jet and (b) the rising CO gas bubbles which carry a thin film of metal into the slag phase.
2. The metal droplets are super saturated with oxygen at the surface in spite of their high carbon content. It is silicon dissolved in metal/droplet which prevents the nucleation of CO bubbles, till the silicon content has decreased to a low level.
3. The metal droplets (supersaturated with oxygen) generate CO at a much faster rate when they come in contact with the gas bubbles which provide additional nucleation sites. Homogeneous nucleation is also possible at very high oxygen super saturation.

The emulsification of slag takes place due to the entrainment of gas and metal droplets in the slag. According to the above mechanism, the decarburization rate should depend strongly on the residence time of metal droplets in the slag phase. If it is considered that the steps 1 and step 3 are very fast due to high turbulence imparted by the top lance and also due to the rising CO gas bubbles, then the step 2 (oxygen transfer to the metal droplets) may become a rate controlling step. In support of this hypothesis, it has been practically observed that slag contains a large number of metal droplets. The carbon content of the droplets is also slightly less than that of the bulk metal. In the middle part of the blow, however, the slag has a much lower FeO content (close to 8% by mass) but the rate of carbon removal is still high. It suggests that another equally fast mechanism of carbon removal exists. It is possible that oxygen rich metal directly under the jet impact zone extends deep into the bulk metal bath and that CO evolves within the metal at numerous heterogeneous sites (viz. on the surface of rising gas bubbles in the metal), or on refractory lining. The rising CO gas bubbles further enhance recirculation of metal, thereby making this particular mechanism of carbon removal more effective.

The laboratory investigations on decarburization kinetics, both for high and low carbon [5, 6] melts, have demonstrated the following aspects.

(a) **For high carbon melts at low partial pressure of oxygen**

1. The rate of decarburization is independent of gas flow rate and is a linear function of oxygen partial pressure.
2. Oxygen activity in the melt is close to equilibrium with the carbon in the melt.
3. Sulphur retards the rate of decarburization due to reduction in the number of sites available for the decarburization. Nitrogen also acts in a similar way due to dissociative adsorption at surface sites.
4. The mechanism of decarburization in Fe-C melt is controlled by dissociative adsorption of oxygen.

5. In the presence of dissolved nitrogen or sulphur, the activation energy increases up to 32–40 Kcal/mole.

(b) **For high carbon melts at high partial pressure of oxygen (similar to that in BOF)**

1. The rate of carbon removal is a linear function of gas flow rate.
2. Temperature has no effect on rate of decarburization.
3. Oxygen activity in bath is at equilibrium with carbon
4. Sulphur and nitrogen have no effect on decarburization rate.
5. Rate controlling step is governed by the reaction $[C] + (FeO) = [Fe] + \{CO\}$

(c) **For low carbon melts**

1. The critical carbon below which the rate of carbon oxidation begins to depend on mass transfer of carbon lies between 0.07% to 0.3%.
2. The critical carbon content does not depend upon the partial pressure of oxygen, temperature and the presence of other elements.
3. Activity of oxygen in the melt is above the equilibrium values associated with the carbon content.

Laboratory investigations on the study of oxidation behaviour of ternary Fe-C-X(X = Si,Mn,P,S) alloy droplets in a ferruginous slag have shown that the laboratory experiments do not correlate at all with the BOF process [13]. For example, the laboratory results suggest that at least in the first half period of refining in BOF, when elements like Si, Mn, P are also present in significant quantity, the dominant reaction is via gas-metal reaction and not via slag-metal reaction. Even in the later part of the blow when emulsion has formed, the gas-metal reaction dominates and the role of the emulsion is merely to reduce the loss of metal through the mouth of vessel.

Dynamic models for actual BOFs have been made with a variety of assumptions. The dynamic control models in the BOF steelmaking process usually rely on the use of waste gas analysis [1–15]. Some approaches are also based upon empirical relationships of various kinetic rates as a function of composition [23]. In most of the models it is assumed that due to abundance of Fe the FeO forms first. The FeO thus formed is reduced by carbon in metal/droplet [8–10]. In one example, it has been suggested that the transport of oxygen in the metal phase is the rate controlling step [11].The reduction rate of FeO has also been calculated by a mixed control model involving gas-phase mass transfer in the slag and the chemical reaction at the metal interface for low sulphur content in metal [7]. In another case, the dynamic model was developed by assuming that transport of oxygen from the jet impact zone to the bulk metal and to the slag-metal interface was the rate controlling step [3, 4]. In a recent work [12], the carbon removal rate was assumed to be controlled by the chemical reaction $[C] + (FeO) = \{CO\} + [Fe]$ and the rate of decarburization was calculated from:

$$\frac{d[C]}{dt} = Vst \cdot A \cdot \exp\left(-\frac{Ea}{RT}\right) \cdot [C] \cdot (FeO)$$

where Ea, [C], (FeO), Vst, T are, respectively, activation energy, bulk carbon molar concentration, bulk FeO molar concentration, steel volume and temperature. Similarly, different equations [23] were applied for simultaneous oxidation of silicon and carbon

$$-\frac{d\mathrm{Si}}{dt} = k1 \cdot [\mathrm{Si}] + k2 \cdot (\mathrm{FeO})$$

$$-\frac{d[\mathrm{C}]}{dt} = k3 \cdot [\mathrm{C}] + k4 \cdot (\mathrm{FeO})$$

The rate constants, $k1$, $k2$, $k3$, $k4$, were determined from actual plant data. The results of this work show that a major proportion of decarburization and desiliconization (up to 90%) takes place in the reaction zone which is set up directly below the jet impact area.

In a sharp contrast with the models already described in literature, the mathematical model developed in the present work is based only on the thermodynamics of reactions wherein the distribution of oxygen between various elements is related to the free energy of formation of oxides. The results show that the BOF process is close to equilibrium in the middle part of the blow and that no assumptions of chemical reaction control and/or mass transport control need to be made. It is however important to set up the model framework such that it reflects the actual process in terms of phases, interfaces and their relative movements with in the BOF. The present paper describes the mathematical formulation as well as the results obtained with the model. The coupled heat and mass transfer model for scrap dissolution is also integrated into the dynamic control model.

Dynamic Model Based upon Thermodynamics of Reactions

The schematic representation of the model is shown in **Figure 1a**. The BOF is divided into several serial and parallel reactors, similar to that suggested in [16–19].

Reactions in metal reactor. In the metal reactor the reactions take place essentially under the jet impact zone. The oxygen supplied by the lance dissolves rapidly into the iron melt up to the solubility limit and thus the oxygen content in the jet impact zone is in equilibrium with pure FeO.

$$O_2 = 2\,[O] \qquad [A]$$

The dissolved oxygen reacts with the dissolved impurities and forms the respective oxides:

$$[C] + [O] = \{CO\} \qquad [B]$$

$$[Fe] + [O] = (FeO) \qquad [C]$$

$$[Si] + 2\,[O] = (SiO_2) \qquad [D]$$

It is assumed that the dissolved oxygen, as also suggested by Wei and Zhu [19], is distributed between the impurities present in the iron melt in the ratio of the free energies of the corresponding reactions. For the reactions B, C and D, free energies are defined as follows; For the sake of simplicity,

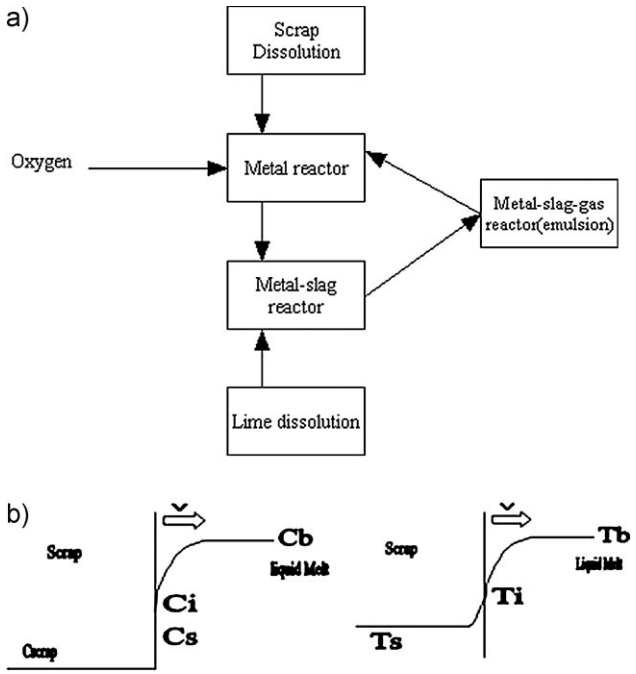

Figure 1. a) Interaction between different modules. b) Schematic diagram of temperature and composition profile in scrap and metal.

the activities of FeO and SiO_2 in the slag phase are calculated by applying the regular solution model [24].

$$\Delta GC1 = \Delta \overset{o}{G} C1 + RT \ln \left[\frac{PCO}{a_C . a_O}\right] \quad (1)$$

$$\Delta GFe1 = \Delta \overset{o}{G} Fe1 + RT \ln \left[\frac{a_{FeO}}{a_O}\right] \quad (2)$$

$$\Delta GSi1 = \Delta \overset{o}{G} Si1 + RT \ln \left[\frac{a_{SiO2}}{a_{Si} . a_O^2}\right] \quad (3)$$

$$x_{C1} = \frac{\Delta GC1}{\Delta GC1 + \Delta GFe1 + \frac{1}{2}\Delta GSi1} \quad (4)$$

$$x_{Si1} = \frac{\frac{1}{2}\Delta GSi1}{\Delta GC1 + \Delta GFe1 + \frac{1}{2}\Delta GSi1} \quad (5)$$

Rate equations, as also suggested by Wei and Zhu [19] are then written as:

$$-\frac{d[\mathrm{C}]}{dt}\frac{Wt\_HM}{100M_C} = \frac{2\eta_C FO2}{22400} x_{C1} \quad (6)$$

$$-2\frac{d[\mathrm{Si}]}{dt}\frac{Wt\_HM}{100M_{Si}} = \frac{2\eta_{Si} FO2}{22400} x_{Si1} \quad (7)$$

It will be shown later that the above distribution ratios can be arrived from the fundamental consideration that driving force for reaction in a system approaching thermodynamic equilibrium is the chemical potential difference.

Reactions in the slag-metal reactor, slag-metal-gas reactor, and lime and scrap dissolution. It is assumed that a fraction of total iron oxide present in the slag is reduced by the following mechanisms:

$$[\mathrm{C}] + (\mathrm{FeO}) = \{\mathrm{CO}\} + [\mathrm{Fe}] \quad [\mathrm{E}]$$

$$[\mathrm{Si}] + 2(\mathrm{FeO}) = (\mathrm{SiO2}) + 2[\mathrm{Fe}] \quad [\mathrm{F}]$$

The distribution of FeO between reactions [E] and [F] is in the ratio of the free energies of the corresponding reactions. For the reactions [E] and [F], the free energies are defined as [19]:

$$\Delta GC2 = \Delta \overset{o}{G} C2 + RT \ln \frac{PCO}{a_C . a_{FeO}} \quad (8)$$

$$\Delta GSi2 = \Delta \overset{o}{G} Si2 + RT \ln \left[\frac{a_{SiO2}}{a_{Si} . a_{FeO}^2}\right] \quad (9)$$

$$x_{C2} = \frac{\Delta GC2}{\Delta GC2 + \frac{1}{2}\Delta GSi2} \quad (10)$$

$$x_{Si2} = \frac{\frac{1}{2}\Delta GSi2}{\Delta GC2 + \frac{1}{2}\Delta GSi2} \quad (11)$$

$$-\frac{d[\mathrm{C}]}{dt}\frac{Wt\_HM}{100M_C} = \frac{2\eta_C FO2}{22400} x_{C2} \quad (12)$$

$$-2\frac{d[\mathrm{Si}]}{dt}\frac{Wt\_HM}{100M_{Si}} = \frac{2\eta_{Si} FO2}{22400} x_{Si2} \quad (13)$$

The efficiency factors (η_C, η_{Si}) are dependent upon concentration and the degree of mixing of the system. For the case of intense mixing of the bath, these factors can be assumed to be unity, implying thermodynamic equilibrium at each step of the process (for the amount of oxygen introduced into to the system). In the initial part of the blow, the mixing gradually increases as the decarburization rate increases. Therefore, the efficiency factor is the function of total mixing energy of the bath arising due to top lance, bottom stirring system and decarburization reactions, which is assumed as follows:

$$efficiency\ factor(\eta_C, \eta_{Si}) \alpha \left(E^o_{total}\right)^n \quad (14)$$

The procedure for calculation of the mixing energy (E^o_{total}) is given in the Appendix. Incorporation of the contribution of mixing is a direct way to represent limiting conditions introduced due to mass transfer control, thereby causing a departure or non-attainment of thermodynamic equilibrium. In the last part of the blow, when carbon falls below a critical value, the first order mass transfer control of carbon is considered in the following way, for the sake of simplicity

$$-\frac{d[\mathrm{C}]}{dt} = k_C . [\mathrm{C}] \quad (15)$$

Emulsion is created due to entrapment of metal droplets ejected from the jet impact zone. It is assumed that the gases are in equilibrium with FeO in the emulsion reactor. Hence,

the post combustion ratio (PCR) inside the vessel is given by:

$$\{CO\} + (FeO) = [Fe] + \{CO2\} \quad [G]$$

$$K_{CO-FeO} = \frac{P_{CO_2}}{P_{CO}.a_{FeO}} \quad (16)$$

The attainment of equilibrium will depend upon the degree of mixing in the emulsion reactor as well. This, in turn, depends upon the mixing caused by decarburization (evolution of CO gas). It is due to this reason that the actual value of PCR is less than the equilibrium value in the initial part of the blow.

Slag volume gradually increases due to dissolution of lime and the formation of oxides (such as SiO_2, FeO). It has been observed in actual practice that the iron oxide rich slag helps to fragment di-calcium silicate layer around the lime particles and also the turbulence in the bath helps to accelerate the lime dissolution kinetics. The rate of lime dissolution is calculated from a simple expression

$$-\frac{dCaO}{dt} = k_{cao}.A_{CaO}.a_{FeO} \quad (17)$$

Scrap dissolution affects the thermal trajectory of the process. The heat and mass transfer equations are coupled together to predict the moving boundary and arrive at the desired solution.

Figure 1b shows the temperature and carbon composition profiles for melting of solid scrap in liquid melt. The following equations (in one dimension) are used to describe the dissolution behavior of scrap

$$\rho Hv + h(Tb-Ti) = \lambda \left.\frac{dT}{dX}\right|_{x=0} \quad [E1]$$

$$\alpha \frac{\partial^2 T_{sc}(x,t)}{\partial x^2} = \frac{\partial T_{sc}(x,t)}{\partial t} \quad [E2]$$

$$v(Ci-Cs) = k(Ci-Cb) \quad [E3]$$

The scrap dissolution model is integrated with the dynamic model of steelmaking at each time step. The accuracy of the results of scrap dissolution model has been validated against an analytical model based on the Green function approach.

Results and Discussion

A comparison of the results of equilibrium okay the dynamic model (based on equilibrium but with efficiency

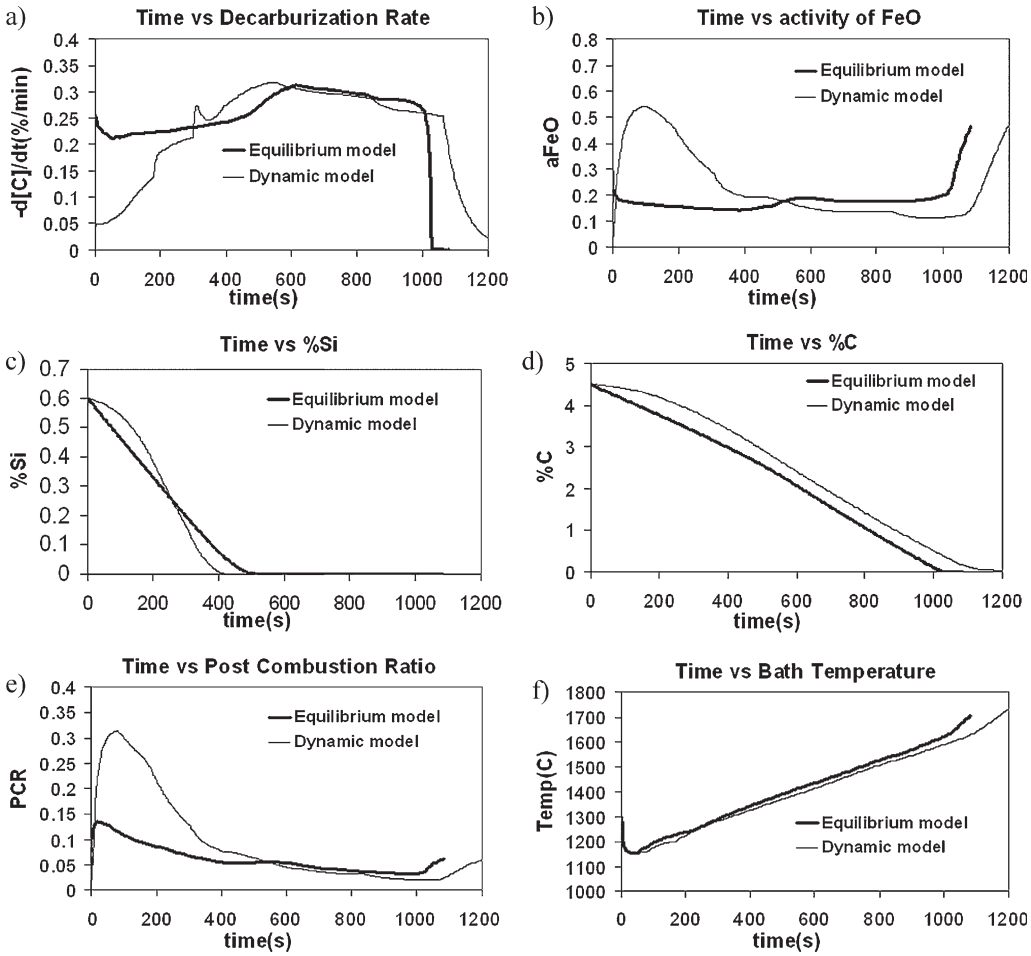

Figure 2. Comparative plots of thermodynamic and real process results.

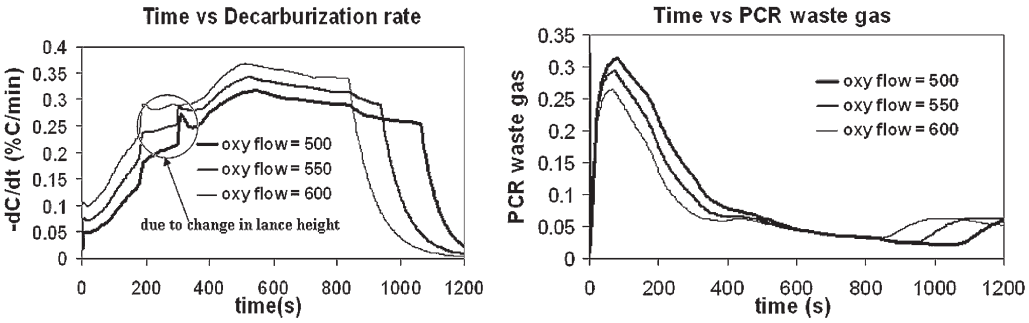

Figure 3. Decarburization rate and post combustion ratios for different oxygen flow rates.

factors suitably incorporated to adapt to the real process) are presented first and then the specific aspects of the success of the dynamic model to predict the specific features of the BOF process (in actual practice) are presented.

Thermodynamics versus the real process. The results of the equilibrium and the dynamic model (for the conditions given in the Appendix) are compared in **Figure 2**. The lines in Figure 2 corresponding to "Dynamic model" do not represent the actual industrial data. The only similarity with the actual process is that the pattern is nearly the same. Thus, the curves corresponding to the "Dynamic model" are actually the lines calculated from the dynamic model. The results clearly demonstrate (Figure 2 a-f) that the actual process deviates from the thermodynamic equilibrium in the initial and the last stages of the process; however the process is close to equilibrium during a major part of the middle blow period (30–70% of blow time). The equilibrium model does not consider the increased loss of iron as dust in the initial stages of the blow, whereas the dynamic model does consider it in an empirical way, and this accounts for the large difference in FeO in slag in the initial stages in Figure 2b. Another anomaly is in the pattern of silicon oxidation. The oxidation rate of silicon predicted by the equilibrium model becomes greater than that predicted by the dynamic model. This is primarily due to the lower temperature of metal in the equilibrium model which renders SiO_2 as more stable, and thus gives lower silicon content in the bath.

Effect of oxygen flow rate. Decarburization rate increases with increase in oxygen flow rate (**Figure 5**).

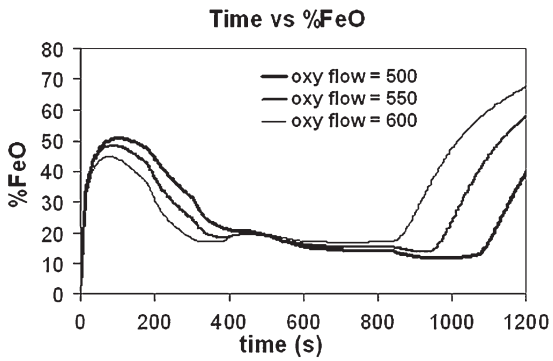

Figure 4. FeO for different oxygen flow rates.

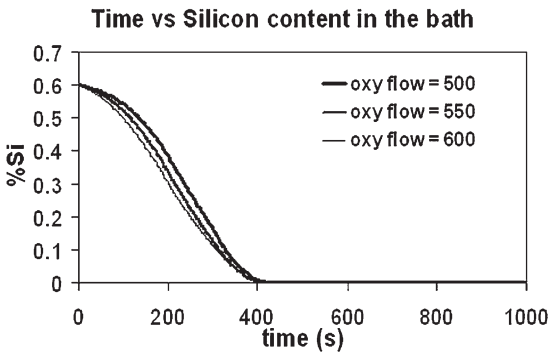

Figure 6. Silicon content at different oxygen flow rates.

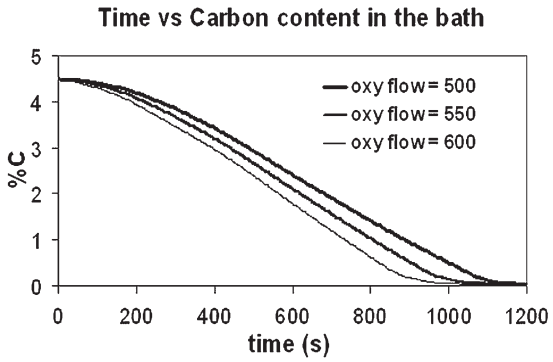

Figure 5. Carbon content at different oxygen flow rates.

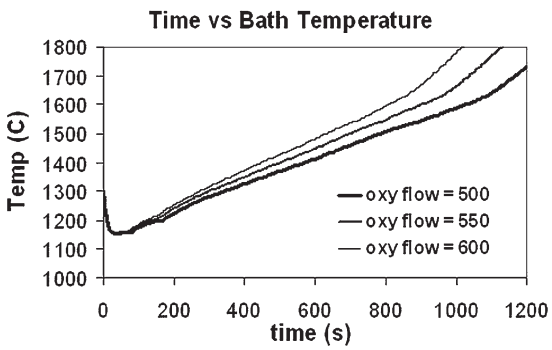

Figure 7. Bath temperature at different oxygen flow rates.

The effect of change in oxygen flow rate is more evident in the middle part of the blow (**Figure 3**). FeO in slag depends upon oxygen flow rate only towards the end of the blow (**Figure 4**). Silicon removal rate increases with oxygen flow rate, though the effect is small (**Figure 6**). Bath temperature increases with oxygen flow rate (**Figure 7**).

Effect of different initial silicon contents. With increase in silicon content of the metal, the time to attain peak decarburization increases (**Figure 8a**). Other factors remaining the same, with lower silicon content of the hot metal, the FeO content of slag is higher in the initial stages of the blow (**Figure 8b**). Higher FeO level during middle of the blow is observed with lower silicon content. The evolution of slag composition for different silicon contents are shown in **Figure 9**.

Effect of scrap size and mix. Due to the presence of a higher proportion of light scrap, the process follows a lower temperature trajectory in the initial stage of the blow. A large proportion of light scrap decreases the bath temperature at the initial stages. In the same way, a very high proportion of heavy scrap increases the bath temperature during the initial part of the blow (**Figure 10**). A higher decarburization rate occurs and the process finishes at an earlier stage when too much heavy scrap is charged (**Figure 11**). A higher post combustion ratio (PCR) is observed in the presence of light scrap in the initial stages of the blow (due to low bath temperature (**Figure 12**). The effect of scrap size on FeO content in slag is also as expected; in the case of light scrap the FeO content of slag in the initial stages is higher (**Figure 13**). The present light scrap cools the bath and thus, if a mixture of light and heavy scrap is charged, then solidification of metal on heavy scrap is enhanced (**Figures 14 and 15**).

Effect of lance height variations. Decarburization rate and FeO level in the slag are plotted for different lance height

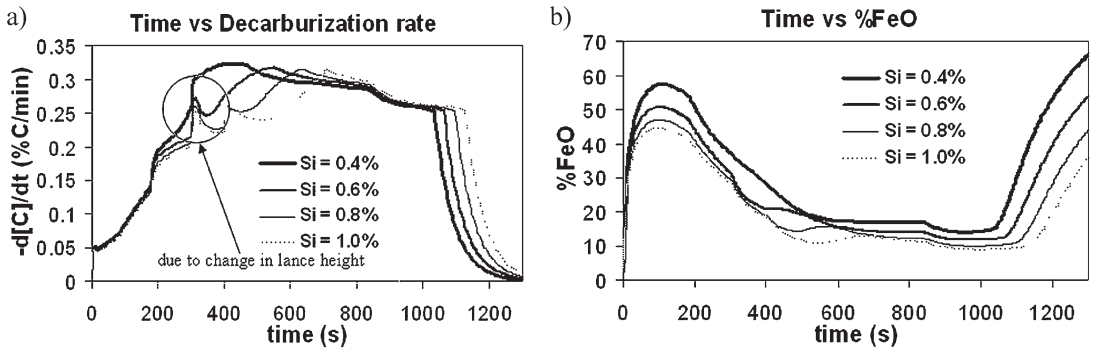

Figure 8. a) Decarburization rate and b) % FeO for different silicon contents for different silicon contents

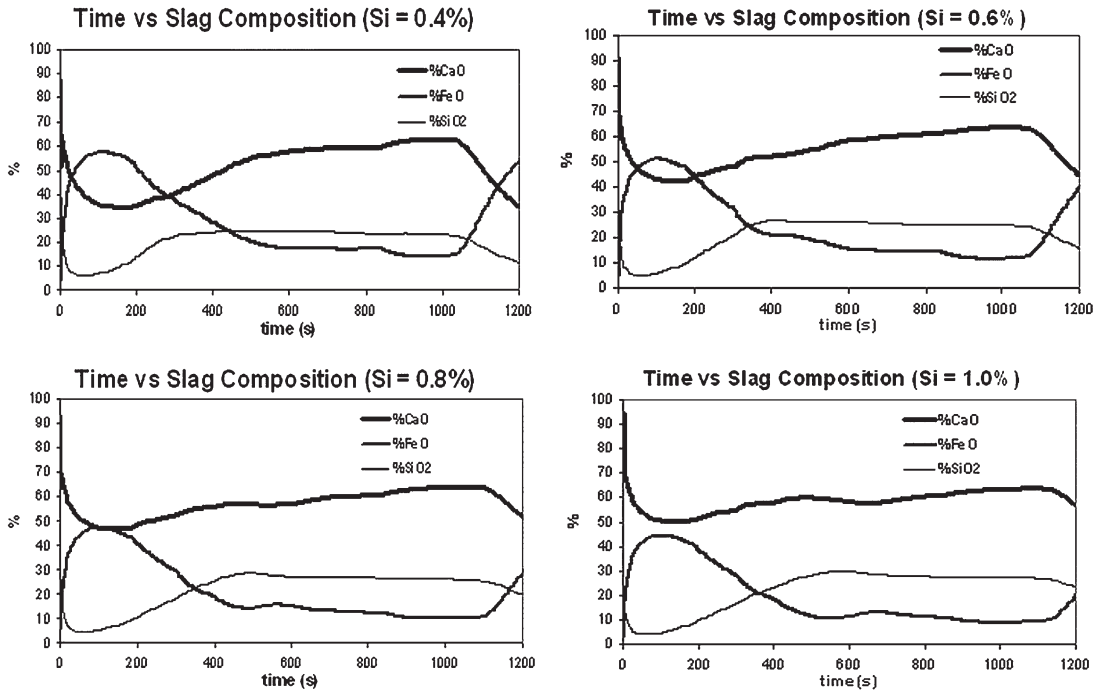

Figure 9. Slag compositions at various initial silicon contents.

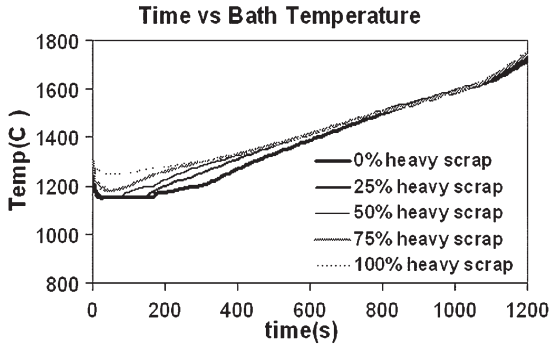

Figure 10. Temperature at different scrap ratios.

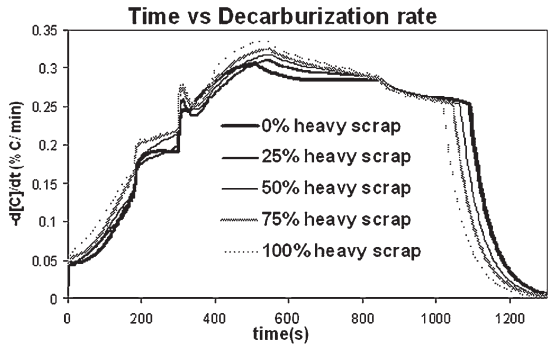

Figure 11. Decarburization rate at different scrap ratios.

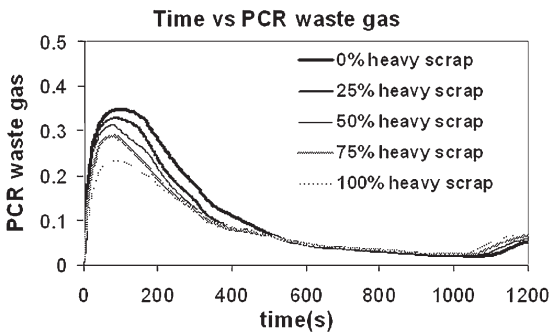

Figure 12. PCR at different scrap ratios.

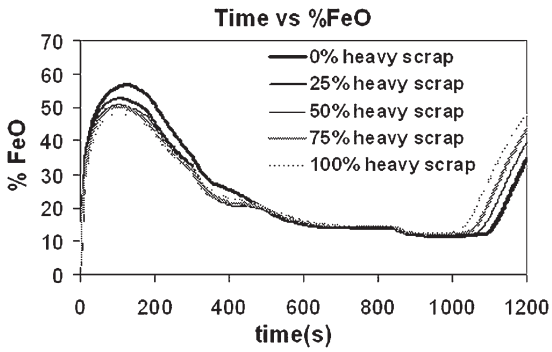

Figure 13. FeO contents at different scrap ratios.

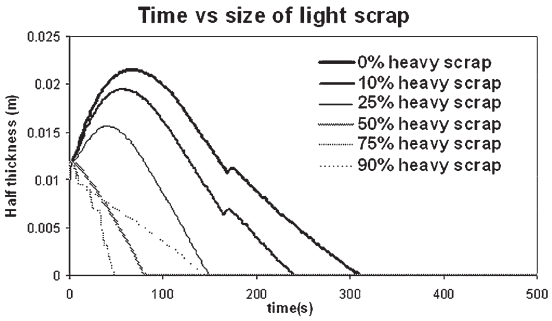

Figure 14. Effect of heavy scrap on the dissolution of light scrap.

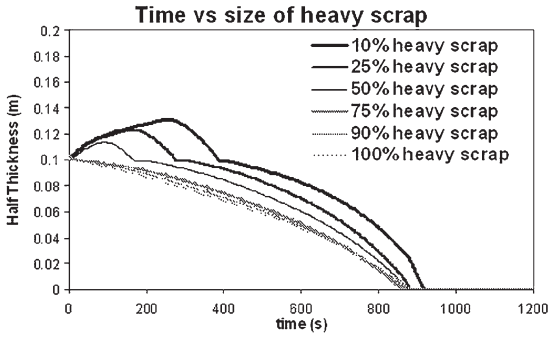

Figure 15. Effect of light scrap on the dissolution of heavy scrap.

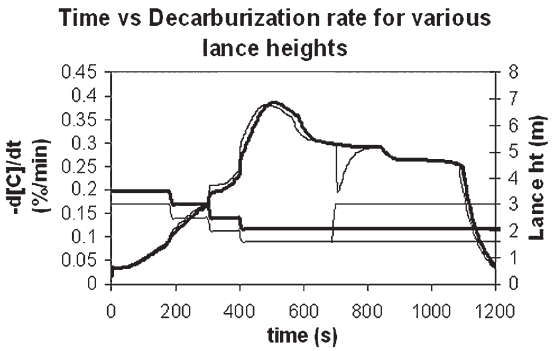

Figure 16. Effect of lance height variation on decarburization rate.

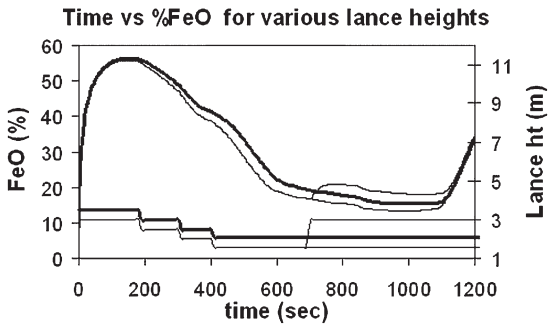

Figure 17. Effect of lance height variation on % FeO.

variations (**Figures 16 and 17**). When the lance height is increased in the middle part of the blow, the FeO in slag rises and the decarburization rate decreases, but only temporarily. Subsequently, the decarburization rate reverts back to the original value (i.e. the value which existed before the increase of the lance height).

Conclusions

The dynamic model developed in this work is based on a fundamental thermodynamic approach. The dynamic model, based on thermodynamic considerations, is able to predict almost all the practically observed features of the BOF process on the shop floor. The predicted results show good agreement with the practical observations on the shop floor. A special feature of the dynamic model is its integration with the scrap dissolution module which takes into account the coupled effects of heat and mass transfer. The model can be used as a simulation tool to study the effect of various parameters. It is proposed to test it further on extensive plant data.

Nomenclature

ρ	Mass density of the scrap, (kg/m^3)
α	Thermal diffusivity of solid scrap, (m^2/s)
h	Heat transfer coefficient between liquid and solid, (W/m^{2}K)
k	Mass transfer coefficient between liquid and solid, (m/s)
v	Moving velocity of the interface (solidification/ melting rate), (m/s)
H	Latent heat of melting (J/kg)
$\lambda =$	Thermal conductivity in the solid steel.
a_C	Activity of carbon in liquid steel
a_O	Activity of dissolved oxygen in liquid steel
a_{Si}	Activity of silicon in liquid steel
a_{FeO}	Activity of FeO in slag (by regular solution model)
a_{SiO_2}	Activity of SiO2 in slag (by regular solution model)
PCO_2	Partial pressure of CO_2
$\Delta GC1$, $\Delta GSi1$, $\Delta GFe1$, $\Delta GC2$, $\Delta GSi2$	Gibbs free energy of respective reactions, (J/mol)
$\Delta \overset{o}{G} C1$, $\Delta \overset{o}{G} Si1$, $\Delta \overset{o}{G} Fe1$, $\Delta \overset{o}{G} C2$, $\Delta \overset{o}{G} Si2$	Standard Gibbs free energy of respective reactions, (J/mol)
Wt_HM	Weight of hot metal, (kg)
M_C, M_{Si}	Molar mass of carbon and silicon (mg/mol)
$FO2$	Oxygen volumetric flow rate (cm^3/s)
T	Temperature of the process, (K)
$K_{CO\text{-}FeO}$	Equilibrium constant for CO-FeO reaction
V_{CaO}	Volume of lime (m^3)
k_{CaO}	Mass transfer coefficient for lime dissolution (m/s)
A_{CaO}	Surface area of lime (m^2)

Appendix

Estimation of total mixing energy in the BOF steelmaking system

The following set of mathematical expressions are used to estimate total mixing energy to the BOF steelmaking system which is considered under combined influence of top lance, bottom stirring flow rate and decarburization reaction [25]:

$$E^0_{top} = 6.32 \times 10^{-7} \cos\varphi \frac{Q_t^3 M}{Wn^2 d_t^3 X}$$

$$Q_{decarb} = \frac{d[C]}{dt} \frac{10^6 \times 22.4 \times 60}{12}$$

$$E^0_{decarb} = 6.18 \times \frac{Q_{decarb} T_l}{W} \left(\ln\left[1 + \frac{\rho g H h\_frac}{p_{atm}}\right] + \left[1 - \frac{T_0}{T_l}\right]\right)$$

$$E^0_b = 6.18 \times \frac{Q_{bottom} T_l}{W} \left(\ln\left[1 + \frac{\rho g H}{p_{atm}}\right] + \left[1 - \frac{T_o}{T_l}\right]\right)$$

$$E^o_{total} = E^o_{top} \times 0.10 + E^o_b + E^0_{decarb}$$

where φ is the angle of the lance tip from vertical, Q_t is oxygen flowrate, W is weight of steel, n is the number of openings of the lance, X is the lance height above metal bath during blowing, H is the average height of the formation of CO bubbles, h_frac is the average depth fraction at which CO bubble formation takes place, d_t is the throat diameter, T_0 is the temperature of the bottom stirring gas at input, T_l is the average temperature of the liquid steel, p_{atm} is the atmospheric pressure and h is the heat transfer coefficient.

Process conditions used in the simulation

Weight of hot metal	150000 kg	Bath depth	1.30 m
Initial scrap to hot metal ratio	0.24	Bottom stirring flow rate	2 Nm^3/min
		(first 30% and last 30% of the blow)	
Light to heavy scrap ratio	0.50		
Initial thickness of light scrap	0.02 m	Blowing Regime is defined as following:	
Initial thickness of heavy scrap	0.20 m	Oxygen flow rate = 500 Nm^3/min	
Initial metal temperature	1573 K	If 0< t < 180 s; Lance height = 2.20 m	
Initial melt carbon content	4.5%	If 180< t < 300 s; Lance height = 2.00 m	
Initial silicon content	0.6%	If 300 < t < 400 s; Lance height = 1.80 m;	
Scrap carbon content	0.10%	If t > 400 s; Lance height = 1.60 m	
Lance angle	14°		
Number of openings in lance	6		
Throat diameter of nozzle	0.0246 m		

References

[1] R. D. Walker, D. Anderson: Iron and Steel, 8 (1972), 403.
[2] J. Szekely: Proceedings of the international conference on kinetics of metallurgical process in steelmaking, 12–14 Oct. 1970, Aachen, Germany.
[3] P. Nilles, F. Merker and H. Voll: Proceedings of the international conference on kinetics of metallurgical process in steelmaking, 12–14 Oct. 1970, Aachen, Germany.
[4] P. Nilles, E. M. Denis: Journal of metal, 21 (1969), No. 7, 74–79.
[5] D. N. Ghosh: Ironmaking and Steelmaking, 2 (1975), No. 1, 36.
[6] J. K. Yoon, J. H. Zong: Metallurgical Transactions, 21B (1990), No. 1, 49.
[7] D. J. Min, R. J. Freuhan: Metallurgical Transactions, 23B (1992), No. 1, 29.
[8] R. Weeks: Proceedings of the international conference on modeling of iron and steelmaking processes, (1972).
[9] R. Middleton and R. Rolls: Proceedings of the international conference on modeling of iron and steelmaking processes, (1972).
[10] E. G. Gisolf, P. Mink, A. Overbosch, R. Boom and B. Deo: Steel Research International, 74 (2003), No. 3, 125.
[11] D. J. Price: Metallurgical chemistry, Proceedings of the International symposium on metallurgical chemistry, held at Brunel University and the National Physical Laboratory on 14–16 July 1971. Published 1972 by H.M.S.O., London
[12] C. Kattenbelt and B. Roffel: Metallurgical Transactions, 39B (2008), No. 5, 764.
[13] T. Gare and G. S. F. Hazeldean: Ironmaking and Steelmaking, 8 (1981), No. 4, 169.
[14] K. C. Chou, U. B. Pal and R. G. Reddy: ISIJ International, 33 (1993), No. 8, 862.
[15] S. Asai and J. Szekley: Metallurgical Transactions, 5 (1974), 651.
[16] M. Modigell, A. Traebert, P. Monheim: AISE Steel Technology, 78 (2001), No. 2, 45.
[17] H. Hollappa, H. Jalkanen: "On the role of slag in oxygen converter process". Proceedings of VII international conference on molten slags fluxes and salts, 25–28 Jan. 2004, Cape Town, South Africa, pp. 71–76.
[18] H. Jalkanen: Acta Metallurgica Slovaca, 13 (2007), No. 3, 434.
[19] J. H. Wei, D. P. Zhu: Metallurgical and Materials Transactions, 33B (2002), No. 1, 111.
[20] P. Costa, B. Canepa: Chemical Engineering Science, 35 (1980), 421.
[21] C. Chigwedu, J. Kempken and W. Pluschkell: "A new approach for the dynamic simulation of the BOF process". Stahl und Eisen, 126 (2006), 25–31.
[22] Y. E. Lee, L. Kolbeinsen: ISIJ International, 47 (2007), No. 5, 764.
[23] B. Deo, V. Balakrishnan: AISTech 2009, conf. Proc., Volume I, ed. by AIST Association for Iron & Steel Technology, Warrendale, USA, 2009.
[24] S. Ban-Ya: ISIJ Int., 33 (1993), No. 1, 2.
[25] K. Nakanishi, T. Fujii, J. Szekely: Ironmaking and Steelmaking, 2 (1975), No. 3, 193.

